Journal of Magnetic Resonance **145,** 334–339 (2000)
doi:10.1006/jmre.2000.2117, available online at http://www.idealibrary.com on IDEAL®

# Sample Restriction Using Magnetic Field Gradients in High-Resolution Solid-State NMR

Patrick Charmont, Anne Lesage, Stefan Steuernagel,* Frank Engelke,* and Lyndon Emsley[1]

*Laboratoire de Stéréochimie et des Interactions Moléculaires, CNRS/ENS, Ecole Normale Supérieure de Lyon, 69364 Lyon, France; and *Bruker Analytik GmbH, Silberstreifen, 76287 Rheinstetten, Germany*

Received February 1, 2000; revised April 5, 2000

**Many solid-state NMR experiments are sensitive to inhomogeneity in the radiofrequency field. We propose a method to restrict the sample volume, in magic angle spinning experiments, using a static magnetic field gradient and a selective pulse. The position of the gradient is calculated for our experimental configuration and we have simulated the effects of selective pulses to determine the excited volume. The resulting sequences are applied to a sample of sodium acetate using frequency-switched Lee–Goldburg proton–proton homonuclear dipolar decoupling. A gain of a factor of 2 on the carbon resolution is experimentally observed.** 

## INTRODUCTION

In solid-state NMR, proton–proton homonuclear dipolar decoupling sequences are interesting for a wide variety of applications (*1, 2*) as diverse as the characterization of proton spectra of coal samples (*3–6*) to their use in carbon-13 spectral editing sequences (*7*). There has been continual development of the first sequences proposed by Lee and Goldburg (*8*) and Waugh *et al.* (*9*), so that there now exist more than 100 different multiple-pulse homonuclear decoupling schemes (*10–14*). An inherent problem with all homonuclear decoupling sequences is that they are more or less sensitive to inhomogeneity in the radiofrequency field. As a result, experiments are usually carried out using samples with a restricted volume, contained in the center of the coil.

However, preparing samples with restricted volumes is often difficult. This is especially so since the ease of decoupling, and thus the degree to which the sample must be restricted, is sample dependent. Ideally one would like to restrict the sample as little as possible in order to maintain a reasonable signal-to-noise ratio. Also, the inserts used to fill the remaining space in the rotor will normally have a different magnetic susceptibility from that of the sample, leading to additional inhomogeneity induced by the sample inserts themselves. This may be reduced somewhat by the use of spherical samples, but spherical samples are so difficult to pack that one seldom actually sees an improvement associated with their use.

In this article we provide an experimental demonstration of how the sample can be restricted using purely spectroscopic techniques. The method is shown to work very well for one of the currently most popular decoupling sequences. Since the method eliminates the need for inserts, it does not suffer from any of the associated difficulties : there are no susceptibility problems, and the effective sample size can be controlled interactively to obtain a useful compromise between sensitivity and resolution.

## GENERATION OF MAGNETIC FIELD GRADIENTS

We propose to restrict the sample using techniques commonly used in magnetic resonance imaging experiments, making use of magnetic field gradients. To restrict the sample volume we apply a field gradient to the sample and then use a selective excitation sequence to excite magnetization only in a certain part of the sample. For cross-polarization magic angle spinning applications the basic experimental setup we use is shown in Fig. 1. In our 2.5-mm-outer-diameter CPMAS probe we can apply a magnetic field gradient to the sample using two opposite Helmholtz coils oriented perpendicular to the rotor axis, as illustrated in Fig. 1a. Curiously enough, this does not lead to a field gradient aligned with the rotor axis (*15*). This can be explained as follows.

In the laboratory frame we can calculate the gradient of the $Z$ component of the magnetic field generated by one of the Helmholtz coils along the three orthogonal directions $X$, $Y$, and $Z$. Note that this is the only component of relevance since the $X$ and $Y$ components do not commute with the main field.

$$B_Z = \frac{\mu_0 I}{4\pi} \int_0^{2\pi} \frac{\lambda R}{r^3}\, d\alpha \qquad [1]$$

[1] To whom correspondence should be addressed. E-mail: Lyndon.Emsley@ens-lyon.fr.



1090-7807/00 $35.00

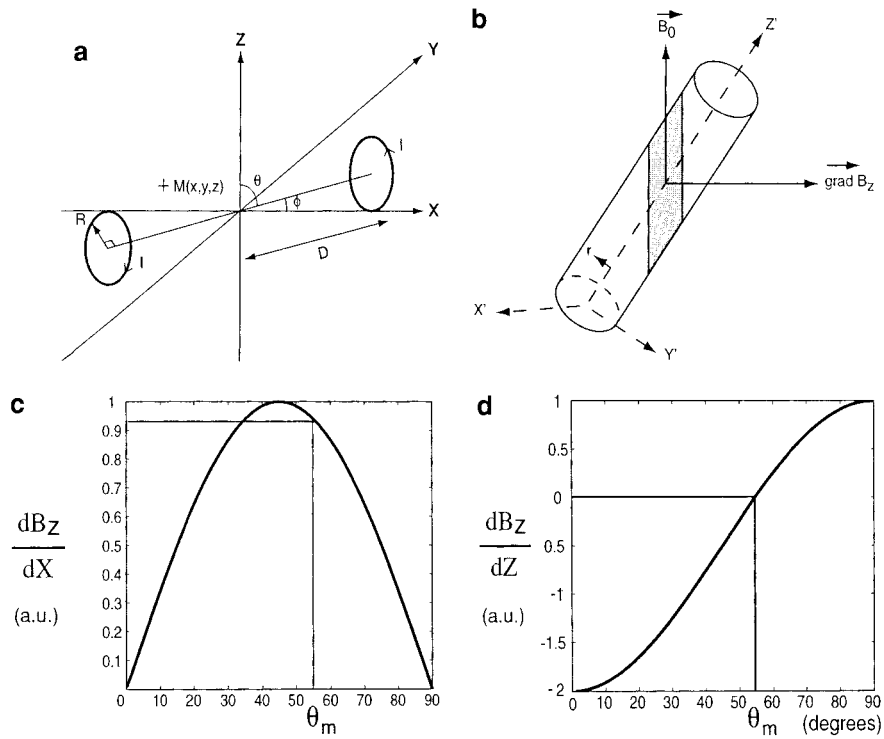


**FIG. 1.** (a) Geometry of the two Helmholtz coils considered in the text. The two anti-Helmholtz coils have opposite currents and are separated by a distance $D = R/2$, which is the definition of a Helmholtz pair. In our CPMAS probe, the coils are oriented at the magic angle, $\theta = \theta_m = 54.7°$. In (b) we show the coordinate system we use, and the geometry of the rotor and the gradient in our 2.5-mm-outer-diameter CPMAS probe. The length of the sample in the whole rotor is 8.5 mm, and the coil is about 6 mm long. The rotor has a 1.5-mm internal diameter. The variation of the gradient of the $Z$ component of the static magnetic field in the $X$ and $Z$ directions as a function of the orientation of the Helmholtz coils, $\theta$, is shown in (c) and (d), respectively. The gradient is calculated at the center of the rotor. For an orientation $\theta$ at the magic angle, the $Z$ component of the gradient is zero, and the $X$ component is almost a maximum.

$$\frac{\partial B_Z}{\partial X} = \frac{\mu_0 IR}{4\pi}\int_0^{2\pi}\frac{\sin\alpha}{r^3} + \frac{3(D\cos\phi - R\sin\alpha\sin\phi - x)\lambda}{r^5}\,d\alpha \quad [2]$$

$$\frac{\partial B_Z}{\partial Y} = \frac{\mu_0 IR}{4\pi}\int_0^{2\pi}\frac{-\cos\alpha\sin\alpha}{r^3} + \frac{3(R\cos\alpha - y)\lambda}{r^5}\,d\alpha \quad [3]$$

$$\frac{\partial B_Z}{\partial Z} = \frac{\mu_0 IR}{4\pi}\int_0^{2\pi} \times\frac{3(D\sin\phi - R\sin\alpha\cos\phi - z)\lambda}{r^5}\,d\alpha. \quad [4]$$

Here $r$ and $\lambda$ are defined by

$$r^2 = (D\cos\phi - R\sin\alpha\sin\phi - X)^2 + (R\cos\alpha - Y)^2 + (D\sin\phi + R\sin\alpha\cos\phi - Z)^2$$

$$\lambda = (R - Y\cos\alpha)\sin\phi - (D\cos\phi - X)\sin\alpha.$$

In order to find the total field gradient generated by both coils, we simply add the equations for the second coil which differ only in that the angle $\phi$ is replaced by $\phi + \pi$.

A complete study of the behavior of the gradient is complicated by the fact that the gradient depends on both the position in the sample and the orientation of the coils. By way of simplification, we can show that the magnitude of the gradient is a maximum at the center of the rotor ($X = Y = Z = 0$)

$$\left(\frac{\partial B_Z}{\partial X}\right)_{\max} = \frac{\mu_0 IR}{4\pi}\frac{9RD}{4(R^2 + D^2)^{5/2}}\sin 2\phi \quad [5]$$

$$\left(\frac{\partial B_Z}{\partial Z}\right)_{\max} = \frac{\mu_0 IR}{4\pi}\frac{9RD}{2(R^2 + D^2)^{5/2}}(1 - 3\cos^2\phi) \quad [6]$$

and that the behavior at the center of the rotor is representative of other points in space. Figure 1 shows the variation of the gradient components as a function of the orientation of the gradient coils. We remark immediately that the $Z$ component of the gradient vanishes at the magic angle, leaving only a relatively large component of the gradient along the $X$ direc-

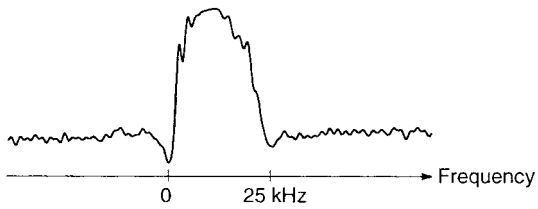


**FIG. 2.** The profile of the whole rotor for a sample of [2-$^{13}$C]sodium acetate. The profile was obtained with a nonselective 90° pulse in the presence of a 30 G/cm gradient along the *X* direction. For the 8.5-mm sample, this yields a linewidth of 25 kHz.

tion. This result is true for any location in the sample, so we conclude that the field gradient will be oriented along the *X* direction if the Helmholtz coils are aligned with the rotor axis.

## SAMPLE RESTRICTION USING MAGNETIC FIELD GRADIENTS

Figure 2 shows the result of recording a carbon-13 spectrum of a singly carbon-13-labeled sample of sodium acetate obtained after a nonselective 90° pulse with acquisition in the presence of this gradient (calibrated to be 30 G/cm). The spectrum is a projection of the spin density onto the axis of the gradient (*16*). Note how the intensity diminishes slightly toward the top of the sample, an effect which reflects the vortexing of the sample. Note that many studies have demonstrated the possibility of doing imaging in MAS experiments (*17–25*). In this paper we are concerned with the effects on *high-resolution spectra.*

Sample restriction equivalent to the use of inserts can be obtained using the pulse sequence shown in Fig. 4a. After the standard cross-polarization step, a nonselective 90° pulse rotates the magnetization to the *Z* axis of the rotating frame. A suitable (amplitude-modulated) selective 90° pulse is then applied in the presence of the gradient to excite magnetization in a slice of the sample. There exist many different pulse shapes to do this (*16, 26, 27*), and we have used one of the simplest, a truncated sinc-shaped pulse of duration $\tau_p$. This type of pulse leads to a large phase dispersion which must be refocused before acquisition, and this is achieved by a nonselective 180° pulse followed by a refocusing gradient. For a sinc-shaped pulse the duration of the refocusing gradient $\tau_{ref} = \tau_p/2$. Note that this sequence is identical to that widely used for slice selection in MRI experiments. The shape of the slice can be modified by changing the pulse shape; e.g., a Gaussian-shaped pulse has a roughly Gaussian excitation profile. The sinc-shaped pulse has a nearly square excitation profile. Questions regarding the excitation bandwidth and slice profile have been widely discussed (*26–28*), and we will not provide further discussion here. The experimental details of our experiments are given in the relevant figure legends. All the pulse sequences used in this work are available from our website (http://www.ens-lyon.fr/STIM/NMR) or upon request to the authors.

There are, however, some interesting questions about the excited volume that arise due to the orientation of the gradient not being colinear with the sample rotation axis (Fig. 1b). As a result the excited volume is not a simple slice perpendicular to the gradient axis. We have calculated the excited volumes by solving the Bloch equations numerically for the time-dependent system under consideration,

$$\frac{dM_x}{dt} = -\Omega M_y \qquad [7a]$$

$$\frac{dM_y}{dt} = \Omega M_x - \omega_1 M_x \qquad [7b]$$

$$\frac{dM_z}{dt} = \omega_1 M_y, \qquad [7c]$$

where

$$\Omega = G\left(\frac{1}{\sqrt{3}}\, r \cos \omega_t t + \sqrt{\frac{2}{3}}\, z'\right), \quad G = 30\text{G/cm} \qquad [8]$$

and

$$\omega_1 = \omega_0 \frac{\sin(\beta(t - t_p/2))}{\beta(t - t_p/2)}, \quad 0 \le t \le t_p. \qquad [9]$$

In Fig. 3 we show the result of these calculations for the 2.5-mm-outer-diameter rotor system we use, as a function of the length of the selective pulse. The figure shows both the form of the region excited and the total signal from the volume. We find that to a very good approximation the volume excited has a cylindrical form with conical "end caps." As a result, except for very small excited volumes, the excited volume depends linearly on the inverse of the pulse length. Thus, we can very easily interactively control the degree of sample restriction by simply varying the selective pulse length.

One might expect, since the gradient axis is not colinear with the rotation, that there should be some interference effects at certain rotor speeds which distort the excited volume. However, for the range of experimental relevance, we have so far not seen any visible variations of the slice profile as a function of rotor frequency, and neither have we seen any effects that could be attributed to the anisotropy of the chemical shift. In contrast, note also that with the currently available gradient strengths, offset effects are difficult to avoid, and represent the principal Achilles' heel of this method. Offset problems will become less and less important as gradient strengths increase.

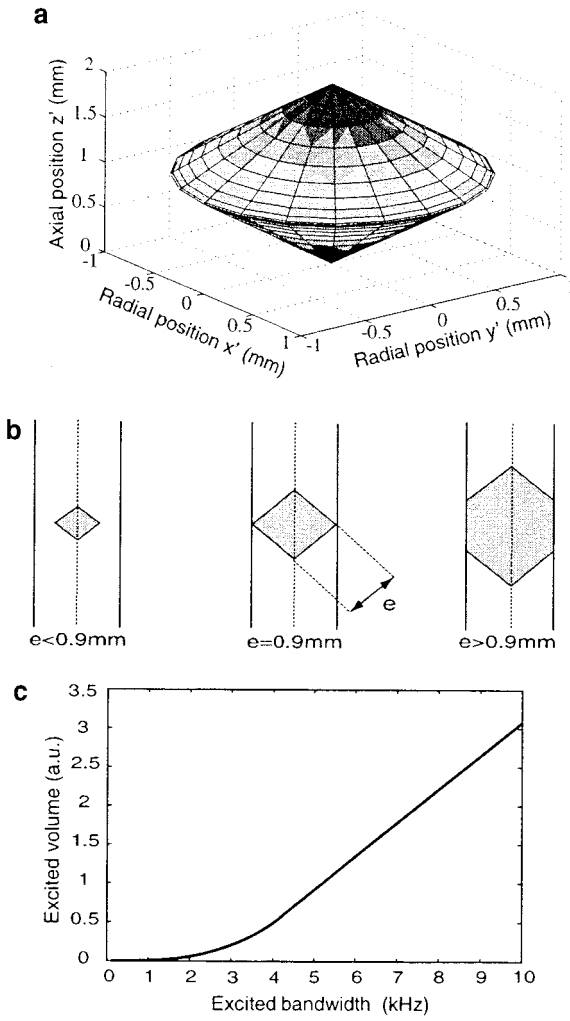


**FIG. 3.** The excited volumes calculated using Eqs. [7] to [9]. The calculations were carried out for a sinc shaped pulse truncated after three zero crossings on either side of the maximum for a rotor with a 1.5-mm internal diameter rotating around the magic angle at a rate of 5 kHz. (a) The result of this calculation for a 5-ms pulse length. Since gradient direction and rotor axis are not parallel, the excited volume is not simply a slice through the rotor, as discussed in the text. (b) Schematic illustration of the variation of the excited volume as a function of the "slice width," which is in turn directly proportional to the inverse of the pulse length. (c) The calculated excited volume as a function of the excitation bandwidth. Except for very small excited widths (less than 0.9 mm), the excited volume is a linear function of the excited width, and thus easy to control.

## APPLICATION TO HOMONUCLEAR DIPOLAR DECOUPLING

After the slice selection step the gradient is removed and, in the sequence of Fig. 4a, acquisition of the carbon-13 free induction decay is carried out in the presence of a homonuclear proton–proton decoupling sequence. We have used the frequency-switched Lee–Goldburg (FSLG) decoupling sequence, introduced by Levitt and co-workers (*29*, *30*), since it is the sequence with which we have recently obtained the best quality spectra (*31*). Using this sequence, under favorable conditions, we have previously demonstrated that one can resolve heteronuclear carbon–proton scalar couplings. Effectively, if the homonuclear proton–proton decoupling is sufficiently good, then the heteronuclear dipolar coupling becomes inhomogeneous in the sense of Maricq and Waugh (*32*) and is removed by magic angle spinning. Thus the only remaining interaction is the scaled heteronuclear carbon–proton scalar coupling which typically has an unscaled value of around 100 Hz (*7*). We find that the degree of resolution of this coupling is a particularly good indirect indicator of the performance of the homonuclear decoupling sequence.

While the FSLG decoupling sequence provides us with our best results, we have noted that sample restriction is very important, and indeed the original paper notes that the main weakness of FSLG is its sensitivity to RF inhomogeneity. Thus

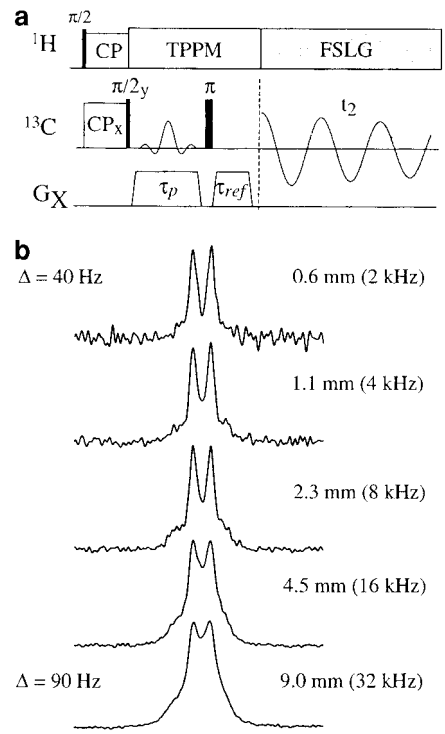


**FIG. 4.** (a) The pulse sequence used to restrict the sample volume. The effect of the sequence is described in the text. (b) The efficiency of FSLG decoupling with varying degrees of sample restriction obtained using the sequence (a). The experiments were performed on a 500-MHz WB Bruker AVANCE spectrometer with a 2.5-mm-outer-diameter double-tuned CP-MAS probe. The spectra show the region of the carbon-13 spectrum containing the $CH_3$ resonance of a sample of polycrystalline [2-$^{13}$C]sodium acetate. FSLG decoupling was achieved using a proton RF field amplitude of 120 kHz. The resolution of the fine structure is directly related to the efficiency of the proton–proton homonuclear decoupling. The excited slice is always centered in the middle of the rotor. For each spectrum, we give the effective slice width in mm and the corresponding excitation bandwidth in kHz. As the slice width diminishes, the decoupling performance is significantly improved, as expected, but the signal-to-noise ratio decreases accordingly.

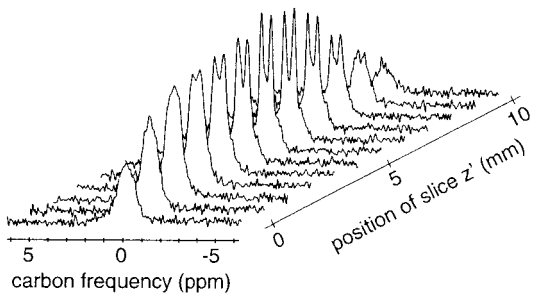


**FIG. 5.** The variation of the performance of FSLG decoupling as a function of the slice position. The spectra were obtained using the same conditions as for Fig. 4b for a 2-mm slice, and the slice position is changed simply by varying the transmitter offset frequency. The decoupling parameters were optimized for the center of the rotor, and they were not reoptimized for each slice. We conclude that, as expected, the homogeneity of the RF field decreases as we move away from the center of the coil.

it provides a very good test case for our sample restriction scheme. The effect of the sequence of Fig. 4a using progressively thinner slices through the sample is shown in Fig. 4b for the methyl carbon resonance in a sample of polycrystalline [2-$^{13}$C]sodium acetate. When the slice thickness contains the whole sample, we see that the heteronuclear scalar coupling is barely resolved. However, a quite spectacular improvement in resolution (i.e., decoupling performance) is observed as the slice thickness is reduced. In the extreme case, with a slice of 0.6 mm (representing 7% of the total sample length) we obtain almost baseline resolution (the carbon-13 full linewidth at half-height going from 90 Hz for a 9-mm slice to 40 Hz for the 0.6-mm slice). Note, of course, that as we reduce progressively the effective sample volume, the sensitivity diminishes accordingly. (There is little we can do about this, but it motivates the development of sequences which are proportionally less sensitive to RF inhomogeneity, thereby requiring less sample restriction for the same result (*33*, *34*).)

As a further demonstration, in Fig. 5 we show a "decoupling profile" of the sample. Each spectrum represents the decoupling performance for a 2-mm slice at different positions in the sample (the slice position is adjusted simply by changing the transmitter offset). As expected we see that the best results are obtained for the slice at the center of the coil. The RF inhomogeneity increases rapidly toward the edges of the coil, and this is reflected in the clear degradation of decoupling performance.

To confirm that the resolution of the carbon-13 fine structure does really reflect the homonuclear decoupling performance, we have measured the proton lineshapes for a 2-mm slice and for the whole sample which yield linewidths of 300 and 400 Hz, respectively. These spectra were obtained indirectly using a through-bond carbon–proton correlation experiment (*31*). As expected, we find that the proton linewidth is narrower in the restricted sample.

## CONCLUSIONS

In conclusion we have demonstrated that sample restriction can be achieved using a simple spectroscopic protocol. The method can be adapted to most solid-state NMR sequences, and should prove useful in many areas. Since the method eliminates the need for inserts, it does not suffer from any of the associated difficulties: there are no susceptibility problems, and the effective sample size can be controlled interactively to obtain a useful compromise between sensitivity and resolution.

For the experimentally very convenient gradient coil geometry that we use, the gradient is not colinear with the rotor axis but it is aligned with the $X$ axis. However, this does not lead to any practical inconvenience in the NMR experiments. The excited volume is linear with the excitation bandwidth, and is thus easy to control, and we have shown that there should be no dependence on the rotation speed for experimentally relevant rotor speeds, so there is only one parameter to adjust.

For the example we show of FSLG homonuclear dipolar decoupling, we have gained over a factor of 2 in resolution using gradient sample restriction.

Finally, we note that this method will also improve $B_0$ inhomogeneity and reduce susceptibility broadening, therefore reducing the linewidth of dilute nuclei such as carbon-13. However, this is usually of little consequence in solid-state NMR (for example, we observe only a few hertz reduction in the carbon linewidth for a CPMAS spectrum of alanine).

## REFERENCES

1. B. C. Gerstein, "CRAMPS," *in* "Encyclopedia of NMR," Wiley, London (1996).
2. M. Pruski, "Cokes," *in* "Encyclopedia of NMR," Wiley, London (1996).
3. D. Michel, M. Pruski, and B. C. Gerstein, *Carbon* **32,** 31 (1994).
4. M. Pruski, D. Michel, and B. C. Gerstein, *Carbon* **32,** 41 (1994).
5. G. E. Maciel, C. E. Bronnimann, and B. L. Hawkins, *Adv. Magn. Reson.* **14,** 125 (1990).
6. B. C. Gerstein, M. Pruski, and D. Michel, "Advances in Coal Spectroscopy" (H. L. C. Meuzelaar, Ed.), Chap. 9, Plenum, New York (1992).
7. A. Lesage, S. Steuernagel, and L. Emsley, Carbon-13 spectral editing in solid state NMR using heteronuclear scalar couplings, *J. Am. Chem. Soc.* **120,** 7095–7100 (1998).
8. M. Lee and W.I. Goldburg, Nuclear magnetic resonance line narrowing by a rotating RF field, *Phys. Rev. A* **140,** 1261–1271 (1965).
9. J. S. Waugh, L. M. Huber, and U. Haeberlen, Approach to high resolution NMR in solids, *Phys. Rev. Lett.* **20,** 180–182 (1968).
10. P. Mansfield, M. J. Orchard, D. C. Richards, and K. H. B. Richards, Symmetrized multipulse NMR experiments in solids: Measurement of the chemical-shift shielding tensor in some compounds, *Phys. Rev. B* **7,** 90–105 (1973).
11. D. P. Burum and W. K. Rhim, Analysis of multiple pulse NMR in solids, *J. Chem. Phys.* **71,** 944–956 (1979).
12. D. P. Burum, M. Linder, and R. R. Ernst, Low-power line

narrowing in solid-state NMR, *J. Magn. Reson.* **44,** 173–188 (1981).

13. D. G. Cory, A new multiple-pulse cycle for homonuclear dipolar decoupling, *J. Magn. Reson.* **94,** 526–534 (1991).
14. J. Virlet, Line narrowing methods in solids, *in* "Encyclopedia of NMR," Wiley, London (1996).
15. W. E. Maas, F. H. Laukien, and D. G. Cory, Gradient, high resolution, magic angle sample spinning NMR, *J. Am. Chem. Soc.* **118,** 13085–13086 (1996).
16. P. G. Morris, "Nuclear Magnetic Resonance Imaging in Medicine and Biology," Clarendon, Oxford (1986).
17. C. Malveau, B. Diter, P. Tekely, and D. Canet, Chemical shift imaging in rotating solids by radiofrequency field gradients, *J. Magn. Reson.* **134,** 171–175 (1998).
18. D. G. Cory, Distorsions in multiple-pulse solid state NMR imaging: Gradient decoupling, time-sequenced second averaging, and over-sampling, *Solid State NMR* **6,** 347–355 (1996).
19. P. Maffei, P. Mutzenhardt, A. Retournand, B. Diter, R. Raulet, J. Brondeau, and D. Canet, NMR spectroscopy by radiofrequency fields gradients, *J. Magn. Reson. A* **107,** 40–49 (1994).
20. Y. Sun, J. Xiong, H. Lock, M. L. Buszko, J. A. Haase, and G. E. Maciel, Solid-state 1H CRAMPS NMR imaging with pulsed rotating magnetic field gradients, *J. Magn. Reson. A* **110,** 1–6 (1994).
21. M. Buszko and G. E. Maciel, Magnetic-field-gradient-coil system for solid-state MAS and CRAMPS NMR imaging, *J. Magn. Reson. A* **107,** 151–157 (1994).
22. J. B. Miller and A. N. Garroway, Carbon-13 refocused gradient imaging of solids, *J. Magn. Reson.* **85,** 255–264 (1989).
23. W. S. Veeman and G. Bijl, NMR imaging of solids with magic angle spinning, *Magn. Reson. Imaging* **10,** 755–763 (1992).
24. E. Gunther, B. Blumich, and H. W. Spiess, Spectroscopic imaging of solids by deuteron magic angle spinning NMR, *Chem. Phys. Lett.* **184,** 251–255 (1991).
25. G. Schauss, B. Blumich, and H. W. Spiess, Conditions for generating rotating gradients in MAS NMR imaging, *J. Magn. Reson.* **95,** 437–441 (1991).
26. R. Freeman, *Chem. Rev.* **91,** 1397 (1991).
27. L. Emsley, Selective pulses, *in* "Encyclopedia of NMR," Wiley, London (1996).
28. P. Borgnat, A. Lesage, S. Caldarelli, and L. Emsley, *J. Magn. Reson. A* **119,** 289 (1996).
29. A. Bielecki, A. C. Kolbert, and M. H. Levitt, Frequency-switched pulse sequences: Homonuclear decoupling and dilute spin NMR in solids, *Chem. Phys. Lett.* **155,** 341–346 (1989).
30. A. Bielecki, A. C. Kolbert, H. J. M. DeGroot, and M. H. Levitt, Frequency-switched Lee–Goldburg sequences in solids, *Adv. Magn. Reson.* **14,** 111–124 (1989).
31. A. Lesage, D. Sakellariou, S. Steuernagel, and L. Emsley, Carbon–proton chemical shift correlation in solid-state NMR by through-bond multiple-quantum spectroscopy, *J. Am. Chem. Soc.* **120,** 13194–13201 (1998).
32. M. M. Maricq and J. S. Waugh, NMR in rotating solids, *J. Chem. Phys.* **70,** 3300–3316 (1979).
33. D. G. Cory and W. E. J. R. Maas, Multiple-pulse cycles for amplitude alignment that are independent of RF inhomogeneity, *J. Magn. Reson. A* **102,** 191–194 (1993).
34. D. Sakellariou, A. Lesage, P. Hodgkinson, and L. Emsley, Homonuclear dipolar decoupling in solid state NMR using continuous phase modulation, *Chem. Phys. Lett.* **319,** 253 (2000).